Direct Speed of Sound Reconstruction from Full-Synthetic Aperture Data with Dual Regularization

Sergio J Sanabria*†, Thurston Brevett*, Rehman Ali*, Arsenii Telichko*, Jeremy Dahl*
Email: sanse@stanford.edu, tbrevett@stanford.edu, rali8@stanford.edu, telichko@stanford.edu, jjdahl@stanford.edu
* Department of Radiology, Stanford University, Stanford, CA, USA
† Deusto Institute of Technology, University of Deusto/Ikerbasque, Basque Foundation for Science, Bilbao, Spain

***Abstract*—Speed-of-sound (SoS) reconstruction in pulse-echo ultrasound can reduce aberrations in imaging and provide quantitative biomarkers for diagnostics. State-of-the-art SoS imaging requires beamformed data for time-delay estimation. This translates either into multi-layered models, where absolute delays t_i at multiple depths are fitted to axial SoS variations, or a perturbation approach, where differential delays between adjacent paths τ_i are used to map SoS heterogeneities. In this work, we remove the beamforming constraint and propose a dual regularization method to combine absolute and differential delays into a generalized SoS reconstruction. Our approach provides quantitative reconstructions in both layered distributions and focal lesions with bias < 2.3 m/s and rmse < 6 m/s. Moreover, it allows scatterer localization with sub-micron resolution. We show experimental results in SoS reconstruction through heterogeneous aberrating layers.**

***Index Terms*—Speed-of-sound, ultrasound computed tomography, regularization, common mid-point, full-synthetic aperture**

I. Introduction

Speed-of-sound (SoS) is defined as the velocity of compressional waves in tissue. SoS is generally approximated with a constant value for soft tissues (≈1540 m/s), while adipose tissue shows lower SoS values (≈1400 m/s) than glandular or fibrous tissues in breast, muscle and liver (> 1500 m/s). Therefore, SoS estimation is an important component in correction of heterogeneous aberrations caused by subcutaneous adipose tissue layers, specially in difficult-to-image patients [1]. SoS also provides a quantitative biomarker to stage conditions related to adipose-accumulation in muscle [2], breast [3] and liver [4], or for breast lesion differentiation [5].

Reconstruction of spatially-resolved SoS distributions from scattering signals with pulse-echo probes has attracted attention in several recent works. [6]–[10]. One class of methods relies on an horizontal layered model of SoS heterogeneity mimicking abdominal layers [6], [7], [11]. A coherence function is maximized to provide average SoS estimates connected to absolute time delay measurements. On the other hand, these models show challenges to reconstruct lateral SoS variations.

This research was fundeding with a NIH Grant R01-EB027100. Sergio J Sanabria was additionally funded by an Ikerbasque Fellowhsip, a grant DTS21/00076 (QUIOMICS) from the Spanish Ministry of Science and Innovation, and a Health Project 2021333036 (ECOFRAIL) from the Basque Governmentfrom , and a Basque Government Health Project 2021333036.

Another class of methods [8]–[10] relies of phase shift estimations among difference paths to reconstruct SoS. These methods provide satisfactory delineaation of focal lesions, but show limitations to reconstruct SoS in layereed geometries, typically requiring a calibration step to estimate global SoS [12]. Overall, all the aforementioned methods require a beamforming step to provide localized time estimates. This in turn introduces a hard prior SoS assumption, which leads to errors in the localization of scattering microstructures and to wavefront distortion.

In this work, we seek to overcome the above limitations by performing SoS reconstruction directly on full-synthetic aperture data, thereby removing the beamforming constraint. We propose a dual regularization method to combine absolute and differential delays into a generalized SoS reconstruction of arbitrary tissue heterogeneity distributions.

II. Theory

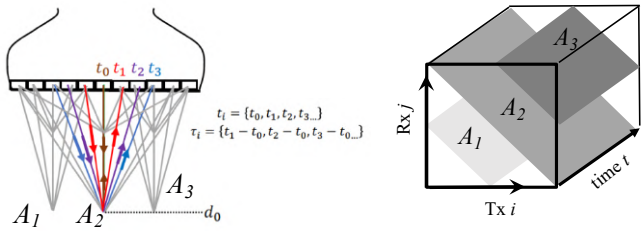

Fig. 1. Tomographic reconstruction of speed-of-sound (SoS) based on time delay estimation from common-mid point gathers (CMPs). Absolute t_i and relative $\tau_i = t_i - t_0$ time delays can be obtained by measuring delays of CMP paths with respect axial path, which is associated to the digitizer delay t_0. CMP sub-apertures $A_1, A_2, A_3, \ldots$ provide overlapping ray paths for tomographic SoS reconstruction.

Given a linear array, we reconstruct SoS directly from full-synthetic aperture datasets (FSA) $V(t, i, j)$, where t is the time axis and i , j are the indices of single crystal transmit-receive events. We estimate time delays based on common mid-point gather signals (CMPs), which consist of k symmetric ray paths $V(t, i-k, i+k)$ with respect to an aperture center i (Fig. 1). CMPs show a high level of redundancy [13], which allow correlation of echos propagating along different paths k for time delay estimation. By constraining propgation to

2022 IEEE International Ultrasonics Symposium (IUS) | 978-1-6654-6657-8/22/$31.00 ©2022 IEEE | DOI: 10.1109/IUS54386.2022.9958718

the axial direction, the echo delay t_0 is defined by the data sampler, while off-axis delays t_k are obtained by referencing CMPs to the axial path. By repeating this approach at multiple digitizer samples and CMP apertures A_1, A_2, A_3, time delay estimates are obtained along anti-diagonal planes A_1, A_2, A_3 of the FSA matrix, which in turn provide overlapping ray paths for tomographic SoS reconstruction.

Due to the lack of focusing of FSA data, CMPs simultaneously capture information from multiple scattering directions S1, S2 (Fig. 2). In a separate contribution, we developed a method for scatter localization by isolating scattering signals from a given azimuth direction [14]. First, we temporally align the scattering direction of interest S1 - here the axial direction- in the FSA dataset. Secondly, we implement a spatio-temporal filter, which removes scattering contributions off-axis, while providing a pass-band for unconstrained estimation in a SoS range representative of soft tissues. Next, we perform time delay estimation by correlating CMP signals $V(i+k, i-k, t)$. with the axial direction $V(i, i, t)$. Here we use zero-normalized cross-correlation (ZNCC) with a kernel window of five wavelengths and three lateral lines, and only store time delay estimates with correlation coefficient $r > 0.7$.

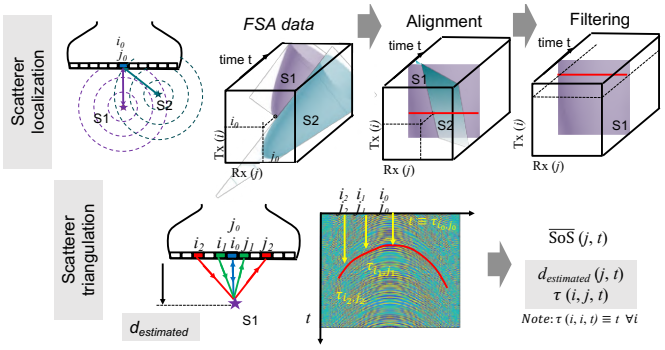

Fig. 2. Localization and triangulation of scatterer S1 based on spatio-temporal filter method described in [14].

Finally, we triangulate the depth location of the scatterer. Given a linear array with pitch p, CMP time delay estimates t_k with respect to the reference digitizer delay t_0, the scattering depths $d(t_0)$ can be estimated as follows:

$$d(t_o) = \sum_{k=1}^{K} \frac{kp}{\sqrt{(t_k/t_0)^2 - 1}} \tag{1}$$

A. Tomographic Reconstruction with Dual Regularization

By defining CMP sub-apertures centered at successive array elements i, overlapping ray paths at multiple tissue depths are traced into a discrete path matrix $\mathbf{L}$. Then absolute delay measurements $\mathbf{t}$ are used as input to solve an inverse ultrasound computed tomography problem:

$$\mathbf{SoS} = (s_{x_l,y_k})^{-1} = \arg\min_{\boldsymbol{s}} ||\mathbf{L}\boldsymbol{s} - \boldsymbol{t}||_n^n + \lambda_1 ||\mathbf{D}\boldsymbol{\sigma}||_n^n \tag{2}$$

where $\mathbf{s}$ the slowness vector, $\mathbf{D}$ a smoothness regularization matrix, n the regularization norm and λ_1 a regularization constant.

Alternatively, we explore the benefits of dropping the reference delays $\mathbf{t_0}$, so that only differential delays $\boldsymbol{\tau}$, with $\tau_i = \{t_1 - t_0, t_2 - t_0, t_3 - t_0\}$, are used in the inverse problem. The path matrix is adjusted accordingly to $\mathbf{\Delta L}$ to account for the differential ray paths.

$$\mathbf{SoS} = (s_{x_l,y_k})^{-1} = \arg\min_{\boldsymbol{s}} ||\mathbf{\Delta L}\boldsymbol{s} - \boldsymbol{\tau}||_n^n + \lambda_1 ||\mathbf{D}\boldsymbol{s}||_n^n \tag{3}$$

Finally, we propose a dual regularization approach, which combines Eq. 2 and Eq. 3 into two separate regularization terms weighted by constants λ_1 and λ_2:

$$\mathbf{SoS} = (s_{x_l,y_k})^{-1} = \arg\min_{\boldsymbol{s}} ||\mathbf{\Delta L}\boldsymbol{s} - \boldsymbol{\tau}||_n^n + \lambda_1 ||\mathbf{D}\boldsymbol{s}||_n^n + \lambda_2 \boldsymbol{s} ||\mathbf{L_{t0}}\boldsymbol{s} - \boldsymbol{t_0}||_n^n \tag{4}$$

In this case we separately weight axial paths $\mathbf{L_{t0}}$ and time samples $\boldsymbol{t_0}$.

For implementation, anisotropically-weighted regularization [15] was applied to $\mathbf{D}$. Without loss of generality, the inverse problem was solved for $n = 2$ least-squares norm with a Tikhonov pseudo-inverse matrix.

III. Materials and Methods

A. Full-wave simulations

Full-wave numerical simulations of ultrasound linear arrays in heterogeneous SoS media were performed using the k-Wave toolbox. Density was adjusted to achieve iso-impedance across the media, including random 5% speckle variations to simulate scattering. FSA datasets were simulated by running N simulations with single element transmits. The grid and temporal steps were 30 μm and 58 ns, respectively.

First, a horizontally-layered medium consisting of four 10 mm thick slabs with distinct SoS was simulated with a 128 element probe with a center frequency of 8 MHz (Fig. 5a - top) and an aperture of 19 mm. A second simulation was run for a homogeneous medium with a circular inclusion of 10 mm diameter using a 128 element probe with 38 mm aperture and a center frequency of 5 MHz (Fig. 5a - bottom).

B. Phantom experiments

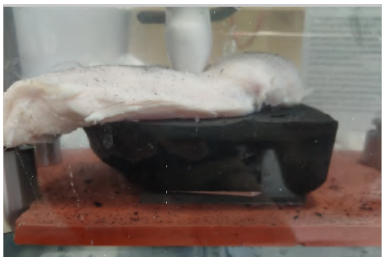

Fig. 3. Experimental setup for homogeneous phantom measurement through aberrating layers. The phantoms were immersed in a water bath during measurement to avoid specular reflections at air inclusions.

Experimental FSA dataset acquisition was performed with a Vantage 128 research ultrasound system (Verasonics Inc., Kirkland, WA, USA). A Hadamard encoding sequence was used to improve the signal-to-noise ratio of the FSA echo traces. Data was acquired with a L12-3v linear array transducer with a center frequency of 8.5 MHz, 192 crystal, a pitch p of 200 µm, and an aperture of 38.4 mm.

Abdominal ultrasound phantoms were manufactured by positioning a 15 mm thick ex-vivo pork layer -simulating aberrations in subcutaneous adipose and musculoskeletal tissues- on top of a set of homogeneous phantoms simulating different stages of liver steatosis [4]. These were manufactured with a mixture of 2-3% agarose, which was mixed with up to 20% of n-propanol to obtain controlled SoS values between 1490 m/s and 1590 m/s. For consistent diffuse scattering pattern, 2% graphite powder was added to all phantoms.

IV. Results and Discussion

Figure 4 show estimated scattering depth locations for the 4-layer medium of Fig. 5a. The depth increments for digitizer samples equi-spaced in time vary with SoS in each layer. Scattering depth was estimated with negligible bias by the proposed triangulation. Applying a median filter corresponding to correlation kernel, the rmse is in submicron range, with 65 nm in the uppermost layer and 217 nm in the bottom layer.

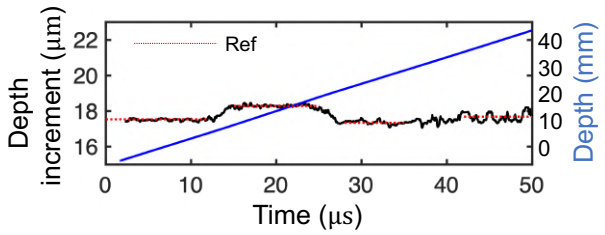

Fig. 4. Scatterer depth estimates for full-wave simulation in Fig. 5a-top. Depth increments agree with reference according to SoS in each layer.

Figure 5 compares SoS reconstruction results with different regularization approaches. Reconstruction with absolute time delays (Fig. 5b) achieves accurate reconstruction of layered geometries with bias < 2 m/s in each of the four layers. In agreement with Fig. 4, the rmse increases from 3 m/s the uppermost layer to 10 m/s in the bottom layer. SoS in the focal lesion is not correctly resolved. This result is comparable to previous coherence-based SoS optimization methods, which are over-constrained to layered structures and show difficulties in discriminating lateral variations. Fig. 5c shows results using differential time shifts and nominal scattering depth estimates assuming a constant SoS of 1540 m/s. In this case, the layered geometry is smeared and the global SoS is biased by 47 m/s from the true value. The inclusion is correctly delineated and its SoS increment with respect to the background (33 m/s) is estimated with error < 5 m/s. By introducing triangulation depth estimates the bias of the global SoS Fig. 5d is reduced to < 1 m/s. On the other hand, due to the limited angular range available along difference paths, the layered geometry is significantly smeared and the rmse goes up to 24 m/s. These results are comparable to previous phase-shift estimation approaches, which are effective in discriminating SoS contrast in lesions but show low axial resolution and typically require a calibration step to estimate global SoS.

Figure 5d shows reconstruction with the proposed dual regularization in Eq. 4. The dual regularization balances the contributions of absolute time delays and differential time shifts, achieving quantitative reconstruction in both layered and focal lesion geometries. The bias and rmse in the layered phantom were 2.3 m/s and 3.0 m/s, respectively, and the inclusion contrast was estimated within an error of < 6 m/s.

Figure 6 shows experimental SoS reconstruction results for the abdominal phantoms. The layers are successfully resolved, allowing quantification of the homogeneous phantom through the aberrating layer. For the investigated 1490-1590 m/s range, the bias and rmse of SoS in the phantom region were 2 m/s and 4.0 m/s, respectively.

Immediately below the aberrating layer in Fig. 6, a discontinuous SoS interface is observed, which may be related to reverberation artifacts and the heterogeneous mixture and adipose and muscle tissue in the pork tissue. The effect of real aberrating layers in CMP phase estimation is further visualized in Fig. 7, which compares simulation a) and experimental b) correlation coefficient for time delay estimations. Average correlation is reduced from 0.97 in simulation data to 0.86 in experimental data. A total of 88% of FSA traces pass the cut-off $r > 0.7$ for delay estimation in the simulation, while 52% passed the cut-off in the phantom experiment. We associate this reduction to deviations from a perfectly diffuse scattering behavior due to reverberation. In the near field coherence is reduced beyond an aperture from the CMP center k_{max}, which increases linearly with tissue depth. The aperture can be modeled with a maximum ray acceptance angle by the array crystals, which was here similarly 30° in a) and 27° in b).

V. Conclusions

Direct SoS reconstruction of generalized tissue geometries is feasible from CMP gathers without beamforming with a dual regularization approach. We illustrate the potential to quantify SoS through phantoms mimicking both abdominal tissue layers and focal inclusions.

References

[1] G. F. Pinton, G. E. Trahey, and J. J. Dahl, "Sources of image degradation in fundamental and harmonic ultrasound imaging using nonlinear, full-wave simulations," *IEEE T Ultrason Ferr*, vol. 58, no. 4, pp. 754–765, 2011.

[2] L. Ruby, A. Kunut, D. N. Nakhostin, F. A. Huber, T. Finkenstaedt *et al.*, "Speed of sound ultrasound: comparison with proton density fat fraction assessed with Dixon MRI for fat content quantification of the lower extremity," *Eur Radiol*, pp. 1–9, 2020.

[3] S. J. Sanabria, O. Goksel, K. Martini, S. Forte, T. Frauenfelder *et al.*, "Breast-density assessment with hand-held ultrasound: A novel biomarker to assess breast cancer risk and to tailor screening?" *Eur Radiol*, vol. 28, no. 8, pp. 3165–3175, 2018.

[4] M. Imbault, A. Faccinetto, B. F. Osmanski, A. Tissier, T. Deffieux *et al.*, "Robust sound speed estimation for ultrasound-based hepatic steatosis assessment," *Phys. Med. Biol.*, vol. 62, no. 9, pp. 3582–3598, apr 2017.

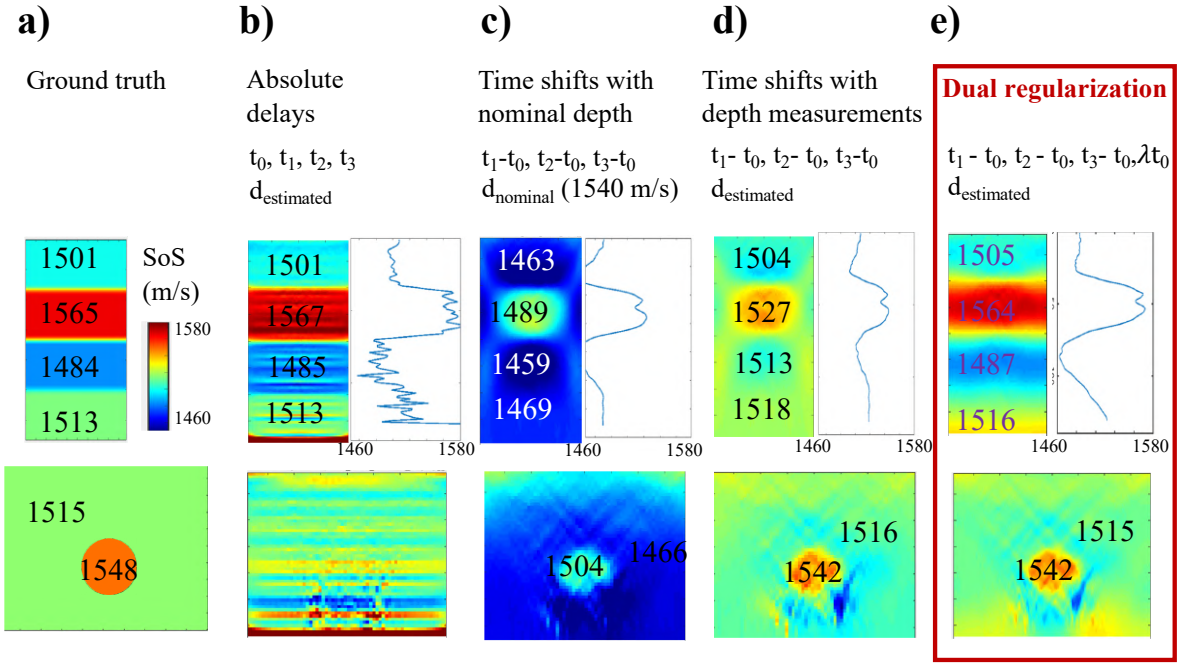

Fig. 5. SoS reconstruction results for full-wave simulations with different geometries and regularization approaches. a) Ground truth for layered media (top) and focal inclusion (bottom). b) Reconstruction with absolute delays (Eq. 2) and estimated scattering depths $d_{\text{estimated}}$ with triangulation (Eq. 1). c) Reconstruction with differential delays (Eq. 3) and nominal distance values with respect to a reference SoS of 1540 m/s. d) Reconstruction with differential delays (Eq. 3) and estimated scattering depths $d_{\text{estimated}}$. e) Proposed dual regularization approach balancing absolute and differential time delays (Eq. 4).

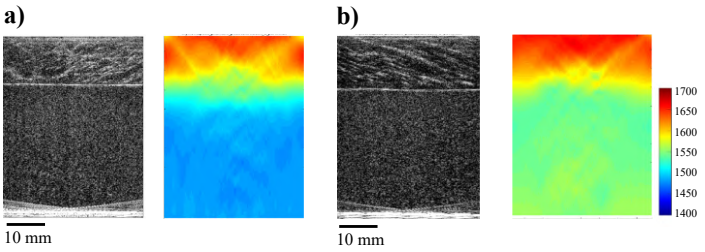

Fig. 6. SoS reconstruction results for homogeneous phantoms through aberrating tissue layer. a) Phantom with SoS of 1490 m/s (left: B-mode, right: SoS reconstruction). b) Phantom with SoS of 1540 m/s.

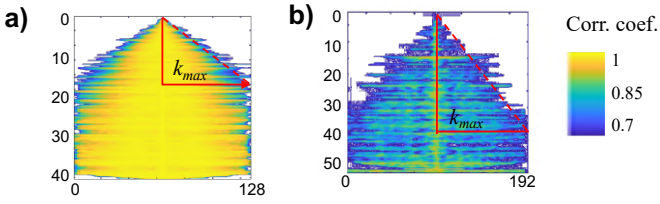

Fig. 7. Correlation coefficient for time delay estimation for a centered CMP aperture. a) shows simulation results (Fig. 5a-top) and b) experimental phantom data (Fig. 6a).

[5] L. Ruby, S. J. Sanabria, K. Martini, K. J. Dedes, Vorburger *et al.*, "Breast Cancer Assessment with Pulse-Echo Speed of Sound Ultrasound from Intrinsic Tissue Reflections: Proof-of-Concept," *Investigative Radiology*, vol. 54, no. 7, pp. 419–427, jul 2019.

[6] M. Jakovljevic, S. Hsieh, R. Ali, G. Chau Loo Kung, D. Hyun *et al.*, "Local speed of sound estimation in tissue using pulse-echo ultrasound: Model-based approach," *J Acoust Soc Am*, vol. 144, no. 1, pp. 254–266, 2018.

[7] R. Ali, T. Brevett, D. Hyung, B. L. L, and D. J, "Distributed Aberration Correction Techniques Based on Tomographic Sound Speed Estimates," *IEEE Transactions on Ultrasonics, Ferroelectrics, and Frequency Control*, vol. 69, no. 5, pp. 1714–1726, 2022.

[8] P. Stähli, M. Kuriakose, M. Frenz, and M. Jaeger, "Improved forward model for quantitative pulse-echo speed-of-sound imaging," *Ultrasonics*, vol. 108, p. 106168, dec 2020.

[9] R. Rau, D. Schweizer, V. Vishnevskiy, and G. O, "Speed-of-sound imaging using diverging waves," *Int J CARS*, vol. 16, pp. 1201–1211, 2021.

[10] S. J. Sanabria, T. Marhenke, R. Furrer, and J. Neuenschwander, "Calculation of volumetric sound field of pulsed air-coupled ultrasound transducers based on single plane measurements," *IEEE Transactions on Ultrasonics, Ferroelectrics and Frequency Control*, vol. 65, no. 1, pp. 72–84, 2018.

[11] A. V. Telichko, R. Ali, T. Brevett, H. Wang, J. G. Vilches-Morue, S. U. Kumar, R. Paulmurugan, and J. J. Dahl, "Noninvasive estimation of local speed of sound by pulse-echo ultrasound in a rat model of nonalcoholic fatty liver," *Phys Med Biol*, vol. 67, no. 1, p. 015007, 2022.

[12] X. Augustin, L. Zhang, and O. Goksel, "Estimating mean speed-of-sound from sequence-dependent geometric disparities," in *IEEE International Ultrasonics Symposium, IUS*, 2021.

[13] "Phase aberration correction using near-field signal redundancy-part i: Principles," *IEEE Transactions on Ultrasonics, Ferroelectrics and Frequency Control*, vol. 44, no. 2, pp. 355–371, 1997.

[14] T. Brevett, S. J. Sanabria, A. Telichko, R. Ali, and J. Dahl, "Speed of sound estimation at multiple angles from common midpoint gathers of non-beamformed data," in *IEEE International Ultrasonics Symposium, IUS*, 2022.

[15] S. J. Sanabria, E. Ozkan, M. Rominger, and O. Goksel, "Spatial domain reconstruction for imaging speed-of-sound with pulse-echo ultrasound: Simulation and in vivo study," *Physics in Medicine and Biology*, vol. 63, no. 21, p. 215015, oct 2018.